First measurement of direct photoproduction of the $a_2(1320)^0$ meson on the proton

A. Celentano,[1] V. Mathieu,[2] A. Pilloni,[3,1] A. Szczepaniak,[4,5,6] K. P. Adhikari,[7] S. Adhikari,[8] M.J. Amaryan,[7] G. Angelini,[9] H. Atac,[10] L. Barion,[11] M. Battaglieri,[12,1] I. Bedlinskiy,[13] Fatiha Benmokhtar,[14] A. Bianconi,[15,16] A.S. Biselli,[17] F. Bossù,[18] S. Boiarinov,[12] W.J. Briscoe,[9] W.K. Brooks,[19,12] D. Bulumulla,[7] V.D. Burkert,[12] D.S. Carman,[12] J.C. Carvajal,[8] P. Chatagnon,[20] T. Chetry,[21] G. Ciullo,[11,22] L. Clark,[23] P.L. Cole,[24,25] M. Contalbrigo,[11] O. Cortes,[9] V. Crede,[26] R. Cruz-Torres,[27] A. D'Angelo,[28,29] N. Dashyan,[30] R. De Vita,[1] M. Defurne,[18] A. Deur,[12] S. Diehl,[31] C. Djalali,[32,33] M. Dugger,[34] R. Dupre,[20] H. Egiyan,[12,35] M. Ehrhart,[36] A. El Alaoui,[19] L. El Fassi,[21,36] L. Elouadrhiri,[12] P. Eugenio,[26] G. Fedotov,[37,*] R. Fersch,[38,39] A. Filippi,[40] G. Gavalian,[12,35] N. Gevorgyan,[30] F.X. Girod,[12,18] D.I. Glazier,[23] W. Gohn,[31,†] E. Golovatch,[37] R.W. Gothe,[33] K.A. Griffioen,[39] M. Guidal,[20] K. Hafidi,[36] H. Hakobyan,[19,30] N. Harrison,[12] M. Hattawy,[7] F. Hauenstein,[7] T.B. Hayward,[39] D. Heddle,[38,12] K. Hicks,[32] A. Hobart,[20] M. Holtrop,[35] Y. Ilieva,[33,9] D.G. Ireland,[23] B.S. Ishkhanov,[37] E.L. Isupov,[37] D. Jenkins,[41] H.S. Jo,[42] K. Joo,[31] S. Joosten,[36] D. Keller,[43,32] M. Khachatryan,[7] A. Khanal,[8] M. Khandaker,[44,‡] A. Kim,[31] C.W. Kim,[9] W. Kim,[42] F.J. Klein,[45] V. Kubarovsky,[12] L. Lanza,[28] M. Leali,[15,16] P. Lenisa,[11,22] K. Livingston,[23] V. Lucherini,[46] I .J .D. MacGregor,[23] D. Marchand,[20] N. Markov,[12,31] L. Marsicano,[1] V. Mascagna,[47,16,§] M.E. McCracken,[48] B. McKinnon,[23] Z.-E. Meziani,[36] M. Mirazita,[46] V. Mokeev,[12] A Movsisyan,[11] E. Munevar,[9,¶] C. Munoz Camacho,[20] P. Nadel-Turonski,[12] K. Neupane,[33] S. Niccolai,[20] G. Niculescu,[49] M. Osipenko,[1] A.I. Ostrovidov,[26] M. Paolone,[10] L.L. Pappalardo,[11,22] R. Paremuzyan,[35] E. Pasyuk,[12] W. Phelps,[9] O. Pogorelko,[13] J.W. Price,[50] Y. Prok,[7,43] M. Ripani,[1] J. Ritman,[51] A. Rizzo,[28,29] G. Rosner,[23] J. Rowley,[32] F. Sabatié,[18] C. Salgado,[44] A. Schmidt,[9] R.A. Schumacher,[48] U. Shrestha,[32] D. Sokan,[23] O. Soto,[46] N. Sparveris,[10] S. Stepanyan,[12] I.I. Strakovsky,[9] S. Strauch,[33] J.A. Tan,[42] N. Tyler,[33] M. Ungaro,[12,31] L. Venturelli,[15,16] H. Voskanyan,[30] E. Voutier,[20] D. Watts,[52] X. Wei,[12] M.H. Wood,[53,33] N. Zachariou,[52] J. Zhang,[43] and Z.W. Zhao[54]

(The CLAS Collaboration)

[1] *INFN, Sezione di Genova, 16146 Genova, Italy*
[2] *Departamento de Fsica Terica and IPARCOS, Universidad Complutense de Madrid, 28040 Madrid, Spain*
[3] *European Centre for Theoretical Studies and Nuclear Physics (ECT*) and Fondazione Bruno Kessler, Strada delle Tabarelle 286, Villazzano (Trento), I-38123, Italy*
[4] *Physics Department, Indiana University, Bloomington, IN 47405, USA*
[5] *Center for Exploration of Energy and Matter, Indiana University, Bloomington, IN 47403, USA*
[6] *Theory Center, Thomas Jefferson National Accelerator Facility, Newport News, VA 23606, USA*
[7] *Old Dominion University, Norfolk, Virginia 23529*
[8] *Florida International University, Miami, Florida 33199*
[9] *The George Washington University, Washington, DC 20052*
[10] *Temple University, Philadelphia, PA 19122*
[11] *INFN, Sezione di Ferrara, 44100 Ferrara, Italy*
[12] *Thomas Jefferson National Accelerator Facility, Newport News, Virginia 23606*
[13] *National Research Centre Kurchatov Institute - ITEP, Moscow, 117259, Russia*
[14] *Duquesne University, 600 Forbes Avenue, Pittsburgh, PA 15282*
[15] *Università degli Studi di Brescia, 25123 Brescia, Italy*
[16] *INFN, Sezione di Pavia, 27100 Pavia, Italy*
[17] *Fairfield University, Fairfield CT 06824*
[18] *IRFU, CEA, Université Paris-Saclay, F-91191 Gif-sur-Yvette, France*
[19] *Universidad Técnica Federico Santa María, Casilla 110-V Valparaíso, Chile*
[20] *Universit'e Paris-Saclay, CNRS/IN2P3, IJCLab, 91405 Orsay, France*
[21] *Mississippi State University, Mississippi State, MS 39762-5167*
[22] *Universita' di Ferrara, 44121 Ferrara, Italy*
[23] *University of Glasgow, Glasgow G12 8QQ, United Kingdom*
[24] *Lamar University, 4400 MLK Blvd, PO Box 10009, Beaumont, Texas 77710*
[25] *Idaho State University, Pocatello, Idaho 83209*
[26] *Florida State University, Tallahassee, Florida 32306*
[27] *Massachusetts Institute of Technology, Cambridge, Massachusetts 02139-4307*
[28] *INFN, Sezione di Roma Tor Vergata, 00133 Rome, Italy*
[29] *Universita' di Roma Tor Vergata, 00133 Rome Italy*
[30] *Yerevan Physics Institute, 375036 Yerevan, Armenia*
[31] *University of Connecticut, Storrs, Connecticut 06269*
[32] *Ohio University, Athens, Ohio 45701*
[33] *University of South Carolina, Columbia, South Carolina 29208*

[34] Arizona State University, Tempe, Arizona 85287-1504
[35] University of New Hampshire, Durham, New Hampshire 03824-3568
[36] Argonne National Laboratory, Argonne, Illinois 60439
[37] Skobeltsyn Institute of Nuclear Physics, Lomonosov Moscow State University, 119234 Moscow, Russia
[38] Christopher Newport University, Newport News, Virginia 23606
[39] College of William and Mary, Williamsburg, Virginia 23187-8795
[40] INFN, Sezione di Torino, 10125 Torino, Italy
[41] Virginia Tech, Blacksburg, Virginia 24061-0435
[42] Kyungpook National University, Daegu 41566, Republic of Korea
[43] University of Virginia, Charlottesville, Virginia 22901
[44] Norfolk State University, Norfolk, Virginia 23504
[45] Catholic University of America, Washington, D.C. 20064
[46] INFN, Laboratori Nazionali di Frascati, 00044 Frascati, Italy
[47] Università degli Studi dell'Insubria, 22100 Como, Italy
[48] Carnegie Mellon University, Pittsburgh, Pennsylvania 15213
[49] James Madison University, Harrisonburg, Virginia 22807
[50] California State University, Dominguez Hills, Carson, CA 90747
[51] Institute fur Kernphysik (Juelich), Juelich, Germany
[52] University of York, York YO10 5DD, United Kingdom
[53] Canisius College, Buffalo, NY
[54] Duke University, Durham, North Carolina 27708-0305

(Dated: April 14, 2020)

We present the first measurement of the exclusive reaction $\gamma p \to a_2(1320)^0\, p$ in the photon energy range 3.5–5.5 GeV and four-momentum transfer squared $0.2 < -t < 2.0\,\mathrm{GeV}^2$. Data were collected with the CEBAF Large Acceptance Spectrometer at the Thomas Jefferson National Accelerator Facility. The neutral a_2 resonance was detected by measuring the reaction $\gamma p \to \pi^0\eta p$ and reconstructing the $\pi^0\eta$ invariant mass. The differential cross section $d\sigma/dt$ was extracted at different beam energies in each $-t$ bin. The most prominent feature of the differential cross section is a dip at $-t \simeq 0.55\,\mathrm{GeV}^2$. This can be well described in the framework of Regge phenomenology, where the exchange degeneracy hypothesis predicts a zero in the reaction amplitude for this value of the four-momentum transfer.

It has been more than forty years since Quantum Chromodynamics (QCD) was postulated as the theory of strong interactions. While much progress has been made in understanding the high energy phenomena through this theory, perturbative methods fail to describe the strong interaction at low energies. A clear understanding of this regime is of key importance, since it corresponds to the dominant manifestation of the strong force in nature, in terms of hadrons that constitute the bulk of the visible mass of the Universe.

Hadron spectroscopy is a valuable tool to experimentally investigate this regime. The measurement of the meson spectrum, in particular searching for exotic states not compatible with the Quark Model, would provide access to the gluonic degrees of freedom that contribute to the quantum numbers of the hadrons. Investigating the properties and interactions of gluons is critical, since their dynamics give rise to the strong interaction that binds the hadrons. In this context, the photoproduction of a $\pi^0\eta$ pair on the proton ($\gamma p \to \pi^0\eta\, p$) is one of the most promising reaction channels: due to the presence of two neutral pseudoscalar mesons in the final state, any P-wave resonance would be unambiguously interpreted as an *exotic*, non $q\overline{q}$ state. So far, only a few results have been reported for this reaction. At low energies, in the fully non-perturbative regime, high-quality cross-section data have been collected by the GRAAL [1], Crystal Ball, TAPS, and A2 [2, 3], and CB-ELSA [4, 5] collaborations. In the multi-GeV photon beam energy range, optimal for meson spectroscopy, instead, no data have been published so far.

Understanding the $\pi\,\eta$ production is crucial for spectroscopy, especially for disentangling new resonance signals from non-resonant backgrounds. In the aforementioned energy regime, the $a_2(1320)$ meson is expected to make the dominant contribution to the $\pi\eta$ invariant-mass spectrum [6]. It can be thus taken as the reference state for a Partial Wave Analysis of this channel, for example allowing for the interpretation of the variations of the $P-D$ phase difference as a signature for the existence of exotic resonances [7, 8]. Photoproduction of the charged a_2 resonance has been measured at SLAC [9–11]. However, to the best of our knowledge the neutral a_2 channel has never been studied in photoproduction.

In this work we report the first measurement of the neutral $a_2(1320)$ meson photoproduction on the proton, for photon beam energies between 3.5 and 5.5 GeV, and four-momentum transferred squared $(-t)$ in the range 0.2–$2.0\,\mathrm{GeV}^2$. The differential cross section $d\sigma/dt$ was obtained by measuring the cross section $d^2\sigma/dtdM$ for the exclusive production of a $\pi^0\eta$ pair on the proton, where M is the two-meson invariant mass, and extracting the contribution of the a_2 resonance in each kinematic bin. The measurement was performed with the

CEBAF Large Acceptance Spectrometer (CLAS) in Hall B at Jefferson Laboratory in a dedicated high-energy, high-statistics run, g12.

In this analysis, all three hadrons in the final state were measured. The π^0 and η were measured by detecting the four photons from their decays, whereas the proton was detected directly. The experiment used a bremsstrahlung photon beam impinging on a 40-cm-long LH_2 target. The photon beam was produced by the interaction of the primary $E_0 = 5.72$ GeV electron beam with a converter of 10^{-4} radiation lengths. A magnetic spectrometer (photon tagger) with energy resolution $0.1\%E_0$ and acceptance in the range $0.2E_0$–$0.95E_0$ was used to tag photons impinging on the target, by measuring the deflected electron momentum [12, 13]. The average electron beam current was approximately 60 nA, resulting in a photon flux of $\sim 4 \cdot 10^7$ γ/s. During the run, the photon flux was measured by sampling the "out-of-time" electron hits in the photon tagger [14].

Outgoing particles were measured with the CLAS detector [15]. This was a large-acceptance spectrometer, based on a toroidal magnet made of six superconducting coils arranged symmetrically around the beamline to produce a field pointing primarily in the azimuthal direction [16]. The coils divided the CLAS detector into six independent magnetic spectrometers (sectors), that shared a common target, trigger and data acquisition system. The momentum of a charged particle was determined from the radius of curvature of its trajectory in the magnetic field as measured by a multi-wire drift-chamber system (DC) [17]. A set of plastic scintillator counters (TOF), installed behind the drift chambers, provided the time of flight of each particle [18]. Particle identification (PID) was performed through the β vs. p technique. The energies and angles of the photons were measured with a lead/scintillator electromagnetic calorimeter (EC), covering polar angles in the range 8°–45°, with energy resolution $\sigma_E/E \simeq 10\%/\sqrt{E(\,\mathrm{GeV})}$, and angular resolution $\sigma_\theta \simeq 10$ mrad [19]. Although CLAS was optimized for charged multi-particle final states, the reaction $\gamma p \to 4\gamma p$ could be measured thanks to the high statistics and the specific setup of the g12 run, with the target moved upstream to maximize the acceptance to multi-meson final states.

The incoming photon was identified based on a coincidence between the vertex times obtained from the photon tagger and from the CLAS detector. The latter was determined by measuring the time of the outgoing charged particles with an array of plastic scintillator counters (ST) surrounding the target [20]. A time coincidence window of ± 1.0 ns was used in this analysis. Due to the large photon flux, a non-negligible fraction of events ($\sim$10%) with more than one tagged photon within the coincidence window was observed. To avoid any bias in the analysis, these events were discarded. This effect was accounted for in the cross-section normalization

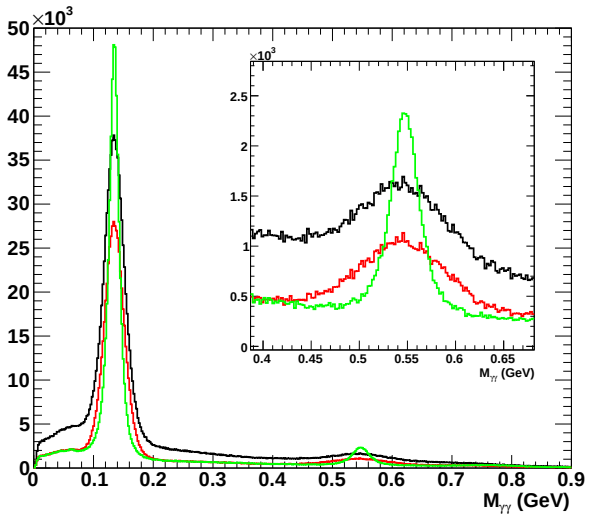

FIG. 1. (Colors online) $M_{\gamma\gamma}$ distribution for events from the reaction $\gamma p \to 4\gamma\, p$. For each event, both combinations $M_{\gamma_1\gamma_2}$ and $M_{\gamma_3\gamma_4}$ are considered, where γ_1 and γ_2 are the photons with the smallest opening angle. Black curve: all events, red curve: events satisfying a 1.86% CL cut. Green curve: events satisfying a 1.86% CL cut, using the corrected 4-momenta from the kinematic fit. The inset shows a zoom in the η mass region.

by including accidental photon tagger hits in the Monte Carlo simulations used to determine the detector acceptance and efficiency, and adopting the same selection procedure.

The g12 experiment used an FPGA-based trigger system, with multiple algorithms implemented in parallel [21]. The main trigger condition required the presence of one charged particle, defined as a coincidence between one TOF hit and one ST hit in the same CLAS sector, and two photons in different CLAS sectors, each defined as an EC hit above a threshold of approximately 100 MeV. The efficiency of the trigger system was evaluated from special minimum bias runs and found to be on average $\varepsilon_{\mathrm{trg}} = 80\%$. To account for the trigger efficiency dependence on the proton impact point on the detector, a trigger efficiency map, as a function of the proton three-momentum, was derived and used to correct the cross-section normalization.

This analysis required a proton and four neutral particles detected, and no other charged particles. The standard g12 procedures, including momentum corrections and fiducial cuts, were applied (see Ref. [21] for a complete description). All neutral particles were considered to be photons, with energies and angles measured by the EC. The selection of events belonging to the exclusive $\gamma p \to 4\gamma p$ reaction was done through a $4C$ kinematic fit (energy and momentum conservation imposed) [22, 23]. To this end, the default g12 covariance matrix (CVM) parameterization for the beam photon and for the final

state proton was used [21]. The final state photons CVM elements, instead, were determined using the reaction $\gamma p \to \pi^0 p \to e^+e^-\gamma p$ [24].

The exclusivity of the final state was ensured by introducing a cut on the kinematic fit confidence level (CL). To optimize this cut, the K kinematic variable, defined as the difference between the missing mass on the proton squared and the four photon invariant mass squared:

$$K = \left(p^\mu_{\rm beam} + p^\mu_{\rm target} - p^\mu_p\right)^2 - \left(\sum_{i=1}^{4} p^\mu_{\gamma_i}\right)^2 , \quad (1)$$

was introduced, where p^μ_j is the measured four momentum of particle j. From energy and momentum conservation, it follows that signal events ($\gamma p \to 4\gamma p$) are distributed around $K = 0$ with a gaussian distribution, while background events ($\gamma p \to 4\gamma p X$) manifest as a tail in the $K > 0$ region. Therefore, the following figure of merit (FOM) was defined:

$$\mathrm{FOM} = \frac{n_s}{\sqrt{n_s + n_b}} , \quad (2)$$

where $n_s/2$ (n_b) was the number of events with $K < 0$ ($K > 0$). The optimal CL cut was determined by maximizing the FOM, and found to be CL = 1.86%. The result of the kinematic fit to the $\gamma p \to 4\gamma\, p$ reaction is shown in Fig. 1. In addition to aiding exclusive event selection, the kinematic fit significantly improves the experimental resolution.

The kinematic fit discussed above was used to select a clean sample of $\gamma p \to 4\gamma p$ exclusive events. The extraction of the $\gamma p \to \pi^0\eta p$ yield from this sample was done as follows. First, the four photons were ordered event-by-event by naming γ_1 and γ_2 those with the smallest opening angle. This algorithm exploits the fact that, due to the lower pion mass, the two photons from the π^0 decay are expected to have, on average, a smaller opening angle than those from η decay. The corresponding efficiency, estimated from Monte Carlo simulations, is approximately 82% [25]. The correlation between the invariant masses of the two photon pairs, $M_{\gamma_1\gamma_2}$ vs. $M_{\gamma_3\gamma_4}$ is shown in Fig. 2. Signal events were identified as those corresponding to the bottom-right cluster centered at $M_{12} = M_{\pi^0}, M_{34} = M_\eta$. A small fraction of events, corresponding to $\simeq 4\%$ of the main signal yield, appear in the opposite combination, and was not considered in the following.

As shown in Fig. 1, after ordering the photons, the $M_{\gamma_3\gamma_4}$ distribution showed a clear peak corresponding to the η, with some residual background underneath coming from exclusive $\gamma p \to 4\gamma p$ events with a different topology. To reject these and extract the signal yield, the ${}_s\mathcal{P}lot$ method was used [26]. This considers that events in the data sample originate from different independent sources and are characterized by a set of kinematic variables that can be split into two components. The method allows

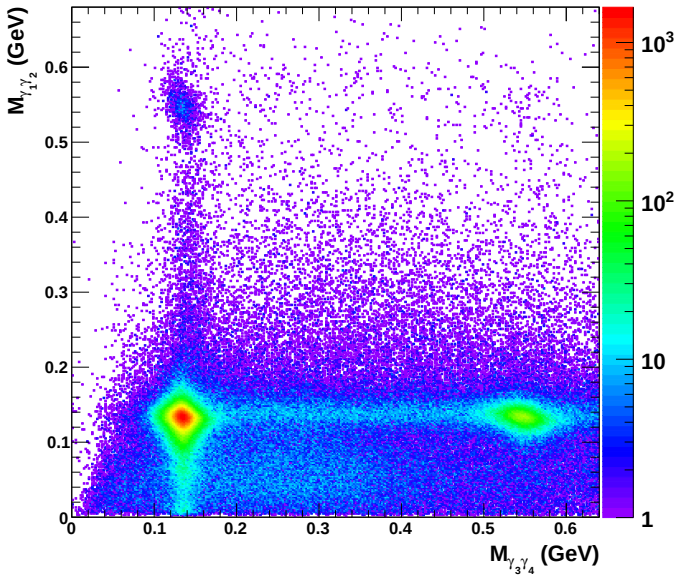

FIG. 2. (Colors online) Correlation between the invariant mass of the two photon pairs for exclusive $\gamma p \to 4\gamma\, p$ events. In each event, γ_1 and γ_2 are the photons with the smallest opening angle. The bottom-right cluster contains signal events from the $\gamma p \to \pi^0\eta p$ reaction. The few events appearing in the opposite photon assignment combination (top-left cluster) were not used in this analysis.

to reconstruct for each event source the distributions of *control variables* from the knowledge of the Probability Density Function (PDF) associated to independent *discriminating variables*. To do so, an extended maximum likelihood fit is performed on the discriminating variables to assign to each event a set of statistical weights, each associated with a specific data source.

In this analysis, the invariant mass $M_{\gamma_3\gamma_4}$ was used as the single discriminating variable, while M and $M_{\gamma_1\gamma_2}$ were used as control variables. Two event sources were assumed: a signal source corresponding to the η meson decay, modeled with a Gaussian PDF with exponential tails, and a background source, parameterized with a polynomial PDF. The nominal fit range was $0.4\,\mathrm{GeV} < M_{\gamma_3\gamma_4} < 0.7\,\mathrm{GeV}$. Events out of this range were rejected. To avoid any correlation between variables that was induced by the kinematic fit, resulting in a bias for the statistical weights, events were first divided into independent M bins, and the ${}_s\mathcal{P}lot$ analysis was applied independently in each of them. A total event yield of $26.2 \cdot 10^3$, defined as the sum of the ${}_s\mathcal{P}lot$ signal weights for all events, was obtained. To assess the quality of the ${}_s\mathcal{P}lot$ method, the $M_{\gamma_1\gamma_2}$ distribution for the signal source was investigated, finding that no residual background was present below the π^0 peak.

The CLAS acceptance and efficiency were evaluated by means of Monte Carlo simulations, based on a GEANT code that included knowledge of the full detector ge-

	N_{bins}	Range	Width
$E_{\rm beam}$	3	2.5-5.5 GeV	1 GeV
$-t$	5	0.2-2.0 GeV^2	Non-uniform. Bin margins: 0.2-0.4-0.7-1.1-1.5-2.0 GeV^2
M	30	0.8-2.3 GeV	50 MeV

TABLE I. Summary of the kinematic bins used in the analysis.

Systematic Uncertainty Source	Magnitude
Target properties	0.5%
Photon flux	5.7%
Trigger efficiency	2.8%
$\eta \to \gamma\gamma$ branching fraction	0.5%
Kinematic fit	Variable, $\sim 3\%$
${}_s\mathcal{P}lot$	Variable, $\sim 4\%$
Acceptance correction	Variable, $\sim 5\%$

TABLE II. Summary of the systematic effects associated with the $\gamma p \to p\pi^0\eta$ differential cross-section measurement. The effects marked as "variable" have a different contribution for each $E_{\rm beam}$, t and M kinematic bin. The typical values are reported.

ometry and a realistic response to traversing particles. Since the extracted differential cross section is integrated over some of the independent kinematic variables (such as the π^0 angles in the Gottfried-Jackson frame), the model used to generate Monte Carlo events had to be as close as possible to the real physical one. To this end, $\gamma p \to \pi^0\eta p$ events were first generated according to a bremsstrahlung photon beam energy spectrum, with a phase-space distribution, and reconstructed through the same procedure used for real data. The result was used to compute the acceptance-corrected event distribution, from which a new Monte Carlo sample was generated. The procedure was iterated until a good agreement between data and Monte Carlo was found. To account for the effect of the analysis procedures in the cross-section normalization, the same methods were applied to Monte Carlo events. These include the exclusion of events with more than one photon in the coincidence time window, the kinematic fit CL cut, the photon ordering algorithm, and the ${}_s\mathcal{P}lot$ method.

The differential cross section $d^2\sigma/dtdM$ is shown in Fig. 3, as a function of M, for three photon-beam energy bins (rows) and five four-momentum transfer bins (columns), as reported in Table I. The error bars report the statistical uncertainty only. This was computed, in each bin, by adding in quadrature the statistical uncertainty on the event yield (equal to the square root of the sum of the ${}_s\mathcal{P}lot$ weights squared) with that on the detector acceptance and efficiency.

The systematic uncertainties in the cross-section determination are summarized in Table II. The first four contributions are connected, respectively, to the uncertainty in the LH_2 target properties (density and length), the absolute photon flux normalization, the trigger system efficiency, and the $\eta \to \gamma\gamma$ branching fraction. The systematic uncertainties associated with the kinematic fit and the ${}_s\mathcal{P}lot$ procedure have been evaluated by considering, in each bin, the relative variation of the cross section for different choices of the kinematic fit CL cut and of the degree of the background polynomial PDF. Finally, the systematic uncertainty on the CLAS acceptance was evaluated by varying the shape of generated events used in the Monte Carlo simulation. The reported total systematic uncertainty of the cross section was obtained by adding in quadrature all individual contributions.

The differential cross section $d^2\sigma/dtdM$ shows two distinctive structures corresponding to the $a_0(980)$ and $a_2(1320)$ resonances. In particular, the a_2 meson is clearly visible as a peak over a smooth background, with the latter decreasing at larger beam energies. The exclusive $a_2(1320)$ photoproduction cross section $d\sigma/dt$ has been extracted in the two largest photon beam energy bins by modeling $d^2\sigma/dtdM$ in the M range 1.1–1.55 GeV as the incoherent sum of a resonance term and a smooth background, including contributions from both non-resonant $\pi^0\eta$ photoproduction and from the residual high-mass tail of the $a_0(980)$ state. The resonance term was written as the product of a $(E_{\rm beam}, -t)$–dependent production coefficient and a Breit-Wigner function that describes the a_2 line shape [27]. The background term was parameterized as an exponentially suppressed zero-order polynomial. The cross-section model was convoluted with the experimental $\pi^0\eta$ invariant-mass resolution, evaluated from Monte Carlo simulations. This ranged from a few MeV at high M values up to $\sim$ 20 MeV at $M \sim 0.8$ GeV. A simultaneous χ^2 fit to all $d^2\sigma/dtdM$ data points was then performed, with a total of 28 free parameters (9 a_2 production coefficients, 9 background polynomial terms, 9 background exponential slopes, and the a_2 mass). In the Breit-Wigner formula, the a_2 mass M_{a_2} was left to vary as a free parameter while the width Γ_{a_2} was fixed to the nominal PDG value, (113.4 ± 1.3) MeV – the effect of this choice was studied and included in the systematic uncertainty. The χ^2/NDF value was $64.3/53 = 1.21$, and the obtained M_{a_2} value was (1309 ± 2) MeV, in very good agreement with the nominal PDG value, (1312.2 ± 2.8) MeV. The fit result is reported for each kinematic bin in Fig. 3 as a red curve, while the black curve shows the a_2 contribution only.

The differential cross section for the reaction $\gamma p \to a_2(1320)^0 p$ was finally obtained by integrating the resonance term in each kinematic bin, accounting for the $a_2 \to \pi^0\eta$ branching fraction, $(14.5 \pm 1.2)\%$ [27]. The results are shown in Fig. 4, where the black (red) points refer to the photon energy range 3.5–4.5 GeV (4.5–5.5 GeV). For each data point, the vertical bar shows the statistical uncertainty, evaluated from the covariance matrix of the χ^2 fit. The colored bands at the bottom show the systematic uncertainty, obtained summing quadratically

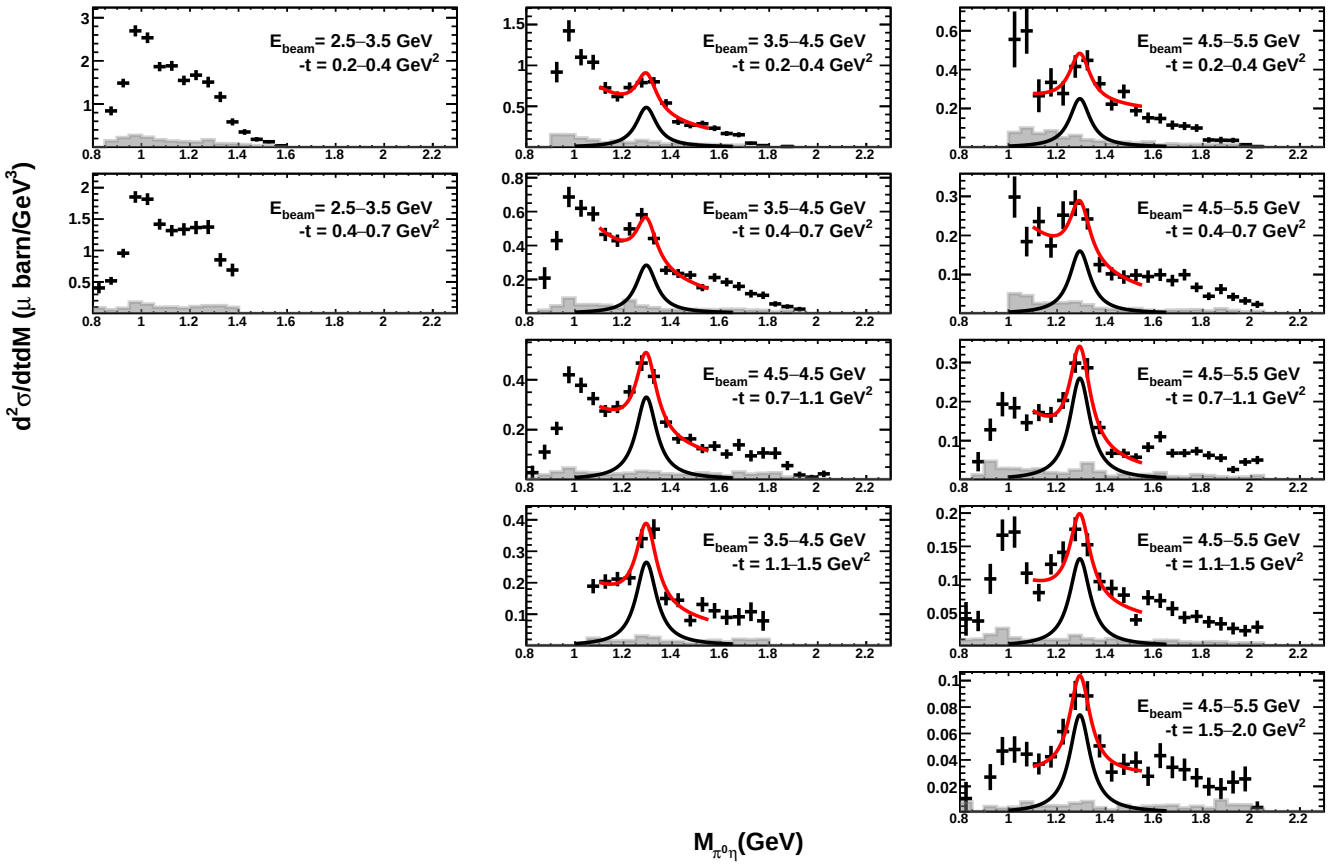

FIG. 3. (Colors online) Differential cross section for the reaction $\gamma p \to \pi^0\eta p$. Each histogram reports the reaction differential cross section $d^2\sigma/dtdM$ as a function of the $\pi^0\eta$ invariant mass, for the specific E_{beam} and $-t$ bin reported in the same panel. The bottom gray-filled area in each panel shows the systematic uncertainty. The red curve is the result from the best fit performed with the model described in the text. The black curve corresponds to the contribution of the a_2 resonance only.

the systematic uncertainty for $d^2\sigma/dtdM$ and that associated with the fit procedure. The latter was evaluated by repeating the fit with different choices of the fit range, the background polynomial order, and the a_2 width – the latter was varied within $\pm 2\sigma$ around the nominal value. The systematic uncertainty was calculated, in each bin, as the RMS of the cross-section data obtained from the different fits.

The most intriguing feature of the $\gamma p \to a_2(1320)\,p$ cross section is the presence of a dip at $-t \simeq 0.55\,\mathrm{GeV}^2$. The hypothesis that this dip, observed simultaneously at both beam energies for the same $-t$ value, was just the effect of a statistical fluctuation, was excluded at 99% CL by comparing the two measured cross-section values to those linearly extrapolated from the nearby data points. The dip can be explained in the context of Regge theory and the specific location of the dip can be traced to the properties of the Regge poles [29]. In Fig. 4, we show the prediction of a model based on a Regge-theory production amplitude parametrization developed by the JPAC Collaboration [28], computed for the two beam energies 4 GeV (black) and 5 GeV (red). The amplitude includes the leading vector trajectories only, which for the production of a neutral $a_2(1320)$ state have the ρ and ω quantum numbers. The magnitude of the amplitude is determined by the coupling of the vector trajectory to γa_2. This is computed using Vector Meson Dominance, from the known $a_2 \to \omega\pi\pi$ width [27], by further assuming that the ρ dominates the $\pi\pi$ state. Regge-resonance duality implies the parameters of Regge amplitudes corresponding to the ρ, ω vector exchanges are closely related to the ones involving the tensor a_2 and f_2 mesons. This is referred to as exchange degeneracy (EXD) [29, 30]. Since there is no scalar meson in the spectrum that could lie on the a_2 trajectory, the residue of the tensor exchange has to vanish when the Regge trajectory $\alpha(t)$ is equal to zero to remove the scalar pole. Vector exchanges, which by EXD share the residues with the tensors, will thus also vanish at $\alpha(t) = 0$, that is at $-t = m^2_{\rho,\omega} \sim 0.55\,\mathrm{GeV}^2$. This leads to an exact zero in the cross section for this value of $-t$. However, subleading Regge poles or cut contributions that correspond to exchanges of heavier mesons or absorption corrections, can turn the zero of the amplitude into the dip observed

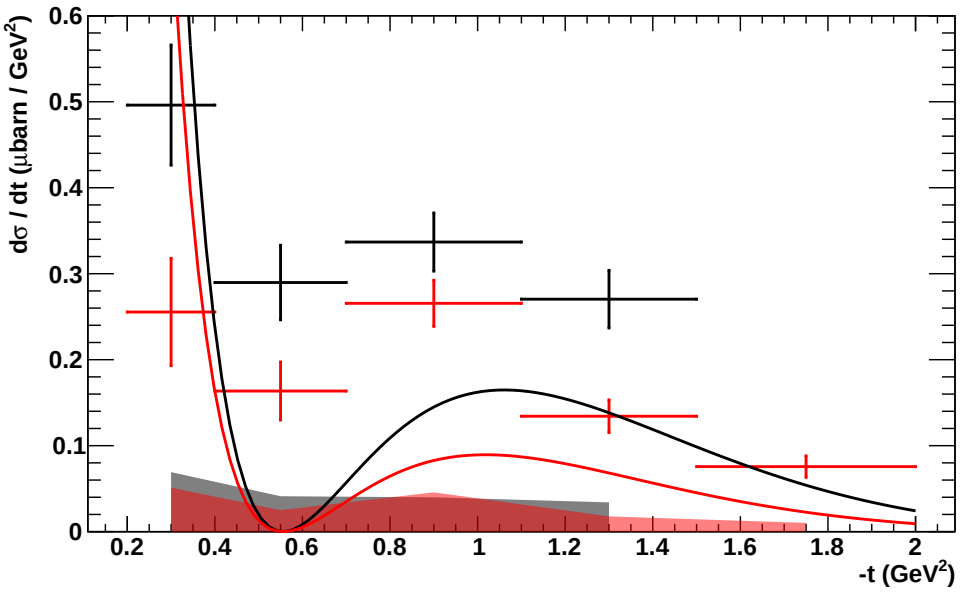

FIG. 4. (Colors online) Differential cross section $d\sigma/dt$ for the reaction $\gamma p \to a_2(1320)p$, for $E_{\rm beam} = 3.5$–$4.5\,\text{GeV}$ (black) and $E_{\rm beam} = 4.5$–$5.5\,\text{GeV}$ (red). The vertical error bars show the statistical uncertainty, whereas horizontal error bars correspond to the $-t$ bins width. The bottom semi-transparent bands show the systematic uncertainty (see text for details). The continuous lines are predictions from the JPAC model [28], computed respectively for a beam energy of 4 GeV (black) and 5 GeV (red).

in data and improve the description at higher $-t$. The good agreement between data and the model prediction demonstrates the effectiveness of a Regge phenomenology based parametrization of the reaction amplitude. This will allow high-statistics photoproduction experiments, *e.g.* CLAS12 [31], GLUEX [32], and BGOOD [33], to properly describe the production of the dominant a_2 resonance in the $\pi^0\eta$ system, using it as a benchmark in the search for exotic states.

In summary, we have measured the reaction $\gamma p \to \pi^0\eta p$ in the photon beam energy range 3.5–5.5 GeV, and for four-momentum transferred squared values between 0.2 and $2.0\,\text{GeV}^2$, extracting for the first time the cross section for the exclusive $a_2(1320)$ photoproduction on the proton. The cross section shows a pronounced dip at $-t \simeq 0.55\,\text{GeV}^2$, which can be explained by the exchange degeneracy hypothesis in the framework of Regge theory. Since the $a_2(1320)^0$ is the most prominent structure present in the $\pi^0\eta$ invariant mass, detailed knowledge of its production cross section is valuable for any assessment of a possible exotic resonance contribution. This measurement will thus help high statistics photoproduction experiments searching for exotic mesons to better understand the $\eta\pi$ mass spectrum.

This work was supported by: the U.S. Department of Energy (DOE), the U.S. National Science Foundation, the U.S. Jeffress Memorial Trust; the Physics and Astronomy Department and the Office of Research and Economic Development at Mississippi State University, the United Kingdom's Science and Technology Facilities Council (STFC), the Italian Istituto Nazionale di Fisica Nucleare; the French Institut National de Physique Nucléaire et de Physique des Particules, the French Centre National de la Recherche Scientifique; and the National Research Foundation of Korea. This material is based upon work supported by the U.S. Department of Energy, Office of Science, Office of Nuclear Physics under contract DE-AC05-06OR23177. V.M. is supported by Comunidad Autónoma de Madrid through Programa de Atracción de Talento Investigador 2018 (Modalidad 1).

* Current address:Ohio University, Athens, Ohio 45701
† Current address:unused, unused
‡ Current address:Idaho State University, Pocatello, Idaho 83209
§ Current address:Università degli Studi di Brescia, 25123 Brescia, Italy
¶ Current address:Thomas Jefferson National Accelerator Facility, Newport News, Virginia 23606

[1] J. Ajaka *et al.*, Phys. Rev. Lett. **100**, 052003 (2008).
[2] V. Kashevarov *et al.* (Crystal Ball at MAMI, TAPS, and A2 Collaborations), Phys. Lett. **B693**, 551 (2010).
[3] V. L. Kashevarov *et al.* (Crystal Ball at MAMI, TAPS, and A2 Collaborations), Eur. Phys. J. **A42**, 141 (2009).
[4] I. Horn *et al.* (CB-ELSA Collaboration), Phys. Rev. Lett. **101**, 202002 (2008).

[5] I. Horn *et al.* (CB-ELSA Collaboration), *Proceedings, 12th International Conference on Hadron spectroscopy (Hadron 2007): Frascati, Italy, October 7-13, 2007*, Eur. Phys. J. **A38**, 173 (2008).

[6] C. Adolph *et al.* (COMPASS Collaboration), Phys. Lett. **B740**, 303 (2015).

[7] A. Rodas *et al.* (JPAC Collaboration), Phys. Rev. Lett. **122**, 042002 (2019).

[8] M. Albrecht *et al.* (Crystal Barrel Collaboration), (2019), arXiv:1909.07091.

[9] G. T. Condo, T. Handler, W. M. Bugg, G. R. Blackett, M. Pisharody, and K. A. Danyo, Phys. Rev. D **48**, 3045 (1993).

[10] G. T. Condo *et al.*, Phys. Rev. D **41**, 3317 (1990).

[11] J. Ballam, G. B. Chadwick, Z. G. T. Guiragossian, A. Levy, M. Menke, P. Seyboth, and G. E. Wolf, Phys. Lett. **30B**, 421 (1969).

[12] D. I. Sober *et al.*, Nucl. Instrum. Meth. **A440**, 263 (2000).

[13] S. Stepanyan, S. Boyarinov, H. Egiyan, L. Guo, D. Dale, M. Gabrielyan, L. Gan, A. Gasparian, A. Glamazdin, B. Mecking, I. Nakagawa, A. Teymurazyan, and M. Wood, Nucl. Instrum. Meth. **A572**, 654 (2007).

[14] J. Ball and E. Pasyuk, *Photon Flux Determination Through Sampling of "out-of-time" hits with the Hall B Photon Tagger*, CLAS-NOTE 2005-002 (2005) `https://www.jlab.org/Hall-B/notes/clas_notes05/2005-002.pdf`.

[15] B. A. Mecking *et al.*, Nucl. Instrum. Meth. **A503**, 513 (2003).

[16] Yu. A. Shishov, Phys. Part. Nucl. **37**, 444 (2006), [Fiz. Elem. Chast. Atom. Yadra 37,843(2006)].

[17] M. D. Mestayer *et al.*, Nucl. Instrum. Meth. **A449**, 81 (2000).

[18] E. S. Smith *et al.*, Nucl. Instrum. Meth. **A432**, 265 (1999).

[19] M. Amarian *et al.*, Nucl. Instrum. Meth. **A460**, 239 (2001).

[20] Y. G. Sharabian, M. Battaglieri, V. Burkert, R. De Vita, L. Elouadrhiri, L. Guo, D. Kashy, V. Kubarovsky, G. Mutchler, M. Ostrick, M. Ripani, P. Rossi, A. Rottura, E. Pasyuk, and D. Weygand, Nucl. Instrum. Meth. **A556**, 246 (2006).

[21] Z. Akbar *et al.*, *g12 Analysis Procedures, Statistics and Systematics*, CLAS-NOTE 2017-002 (2017) `https://misportal.jlab.org/ul/Physics/Hall-B/clas/viewFile.cfm/2017-002.pdf?documentId=756`.

[22] D. Keller, *Techniques in kinematic fitting*, CLAS-NOTE 2010-015 (2010) `https://misportal.jlab.org/ul/Physics/Hall-B/clas/viewFile.cfm/2010-015.pdf?documentId=614`.

[23] M. Williams and C. A. Meyer, *Kinematic Fitting in CLAS*, CLAS-NOTE 2003-017 (2003) `https://www.jlab.org/Hall-B/notes/clas_notes03/03-017.pdf`.

[24] M. C. Kunkel *et al.* (CLAS Collaboration), Phys. Rev. C **98**, 015207 (2018).

[25] A. Celentano, *The Forward Tagger detector for CLAS12 at Jefferson Laboratory and the MesonEx experiment*, Ph.D. thesis, Università degli Studi di Genova (2014).

[26] M. Pivk and F. R. Le Diberder, Nucl. Instrum. Meth. **A555**, 356 (2005).

[27] M. Tanabashi *et al.* (Particle Data Group), Phys. Rev. D **98**, 030001 (2018).

[28] JPAC Collaboration, Private communication.

[29] A. C. Irving and R. P. Worden, Phys. Rept. **34**, 117 (1977).

[30] J. Mandula, J. Weyers, and G. Zweig, Ann. Rev. Nucl. Part. Sci. **20**, 289 (1970).

[31] A. Celentano, Journal of Physics: Conference Series **424**, 012007 (2013).

[32] A. Austregesilo (GlueX Collaboration), *Proceedings, 21st International Conference on Particles and Nuclei (PANIC 17): Beijing, China, September 1-5, 2017*, Int. J. Mod. Phys. Conf. Ser. **46**, 1860029 (2018).

[33] S. Alef *et al.* (BGOOD Collaboration), "The BGOOD experimental setup at ELSA," (2019), arXiv:1910.11939.